Rate Calculations for the Focal Plane Scanner for the Q-weak Experiment

David J. Harrison

University of Winnipeg
Physics Department
Honors Thesis
Supervisor: Dr. J. Martin

April 24, 2008

Abstract

The Q-weak experiment is a low-energy parity violation electron-proton scattering experiment which is designed to measure the weak charge of the proton ($Q_w^p = 1 - 4\sin^2\theta_w$) with a combined experimental error of 4%. The standard model predicts Q_w^p based on the running of $\sin^2\theta_w$ with four-momentum transfer Q^2. In the Q-weak experiment, 1.165 GeV electrons in a 180 μA beam scatter from a liquid hydrogen target. Elastically scattered electrons are focused by a toroidal magnet onto 8 integrating quartz bar detectors. Track reconstruction in the experiment is performed at currents of 1-100 nA which provides a measurement of Q^2. A focal plane quartz scanner device will be used in the experiment to extrapolate the value of Q^2 from these low beam current calibration runs to the higher current parity violation runs at 180 μA. The scanner can also be used in tracking and background measurements. The scanner system counts coincidences observed in two overlapping 2cm by 1cm quartz radiators attached to optically isolated cylindrical light guides placed at a 90° angle to one another. To understand systematic effects in the scanner which could effect the extrapolation over beam current, a Monte Carlo simulation based on a custom c++ code was performed. Results of the simulation will be discussed.

Supervisor: Dr. J. Martin
Thesis Committee: Dr. S. Dannefaer and Dr. R. Kobes

Contents

List of Figures

Chapter 1

Introduction

1.1 Overview of the Standard Model

The standard model of particle physics is a well tested model which describes interactions between particles. The model breaks up matter into two main categories, the quarks and the leptons. There are six different flavors of quarks in the standard model split into three generations. First generation quarks are the up and down, second generation are the strange and charm quarks and third generation quarks are the top and bottom. Leptons are also categorized into three flavors: the electron and the electron neutrino, the muon and muon neutrino and the tau and tau neutrino. All the particles in the standard model have anti-particle partners with the same mass and opposite charge. The interactions of these particles are described using the following force mediators: photon (γ), gluon (g) and the $W+$, W^- and Z^0 bosons.

All matter is made up of the fundamental particles. Quarks can combine together in two ways: mesons and baryons. A meson is a quark (q) anti-quark ($\bar{q}$) pair. A baryon is a combination of three quarks. Combining quark compositions with leptons creates atoms and molecules.

Though very successful, the standard model does not predict everything and there are gaps in it's ability to describe the subatomic world. There have been many experiments which test various aspects of the standard model by measuring parameters with great precision. By measuring parameters with great precision recognition of possible deviations from standard model predictions are possible, or, barring that, tight constraints will be created on theories of physics beyond the standard model. One parameter which has a firm prediction based on the standard model is the weak mixing angle (θ_w). This parameter is an essential component of the Glashow-Weinberg-Salam (GWS) model which unifies the electromagnetic and weak forces into the electroweak force.

The GWS model was first published in 1967 [2]. The theory suggests the weak coupling constants are linked to the electromagnetic coupling constant (g_e) (which in appropriate units is the charge of the positron) by the following relations [2].

$$g_w = \frac{g_e}{\sin\theta_w}, \qquad g_z = \frac{g_e}{\sin\theta_w \cos\theta_w} \tag{1.1}$$

Further to relating the coupling constants GWS shows that two neutral states, the B and W, "mix" together to produce a massless linear combination the photon (γ) equation 1.2 and a massive orthogonal combination the Z^0 boson equation 1.3 [2].

$$A = B\cos\theta_w + W\sin\theta_w \tag{1.2}$$

$$Z = -B\sin\theta_w + W\cos\theta_w \tag{1.3}$$

The standard model also predicts that the weak mixing angle, or, equivalently, $\sin^2\theta_w$ varies or "runs" with the energy scale (Q). The reason for the dependence of $\sin^2\theta_w$ on Q is that the coupling constants g_e, g_w and g_z depend on the distance between the particles. To explain this, consider the process of vacuum polarization, in which virtual positron-electron pairs are created in the vacuum. A Feynman diagram representative of vacuum polarization is displayed in Figure 1.1. The virtual pairs tend to shield the bare charge and in doing so reduce the coupling constant. Corrections such as this cause the weak charge and hence $\sin^2\theta_w$ to vary with Q.

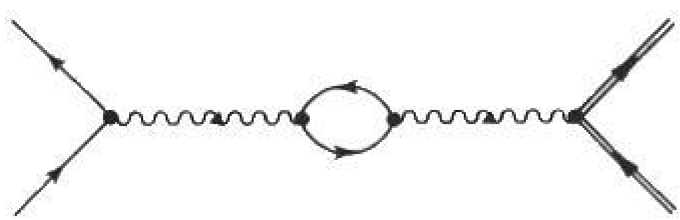

Figure 1.1: Feynman diagram for electromagnetic vacuum polarization [2]

Figure 1.2 shows the running of $\sin^2\theta_w$ with Q. Black data points indicate previous measurements of $\sin^2\theta_w$. Previous measurements come from atomic parity violation (APV), parity violating (PV) e-e (Moller) scattering (SLAC E-158), deep inelastic neutrino-nucleus scattering (NuTeV), and from Z^0 pole measurements (LEP+SLC)[6]. The (Q_w^p), labeled with a red dot, is the value which is to be determined by the Q-weak experiment and the error bar corresponds to a successful determination of (Q_w^p) at the 4% level (combined statistical and systematic errors). The blue line is a calculation of the running of $\sin^2\theta_w$ and is the prediction based on the standard model [6]. The error in the prediction is represented by the thickness of the line. It is evident from the thickness of the line that the confidence in the standard model prediction is high.

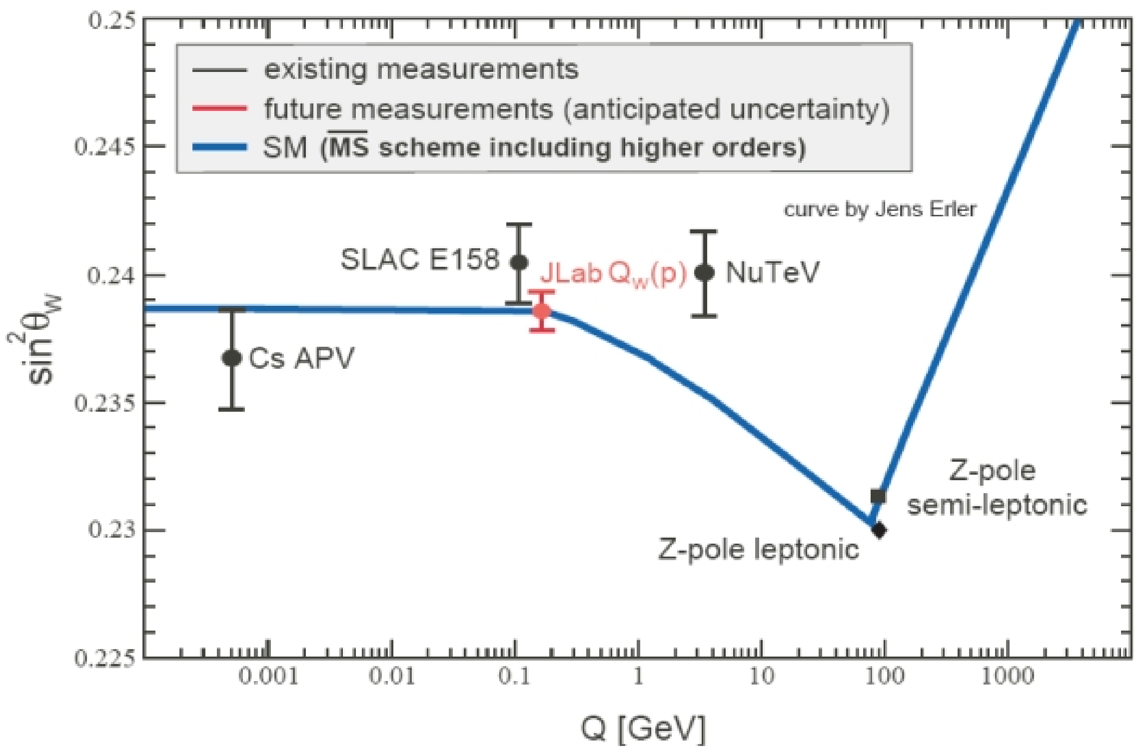

Figure 1.2: The running of $\sin^2\theta_w$

1.2 Electron-Proton Scattering

1.2.1 Kinematics

The tool which will be used by the Q-weak experiment in measuring $\sin^2\theta_w$ is elastic electron-proton scattering and a brief outline of it's theoretical treatment is provided here. Every physical interaction can be drawn as a series of schematic Feynman diagrams. A first order Feynman diagram for electromagnetic electron-proton scattering is shown in Figure 1.3[2]. The vertical axis represents time and the horizontal axis position. The diagram shows an electron with four-momentum p_1 and proton with four-momentum p_2 entering and moving toward each other, they then exchange a virtual photon with four-momentum q and leave moving away from each other with four-momenta p_3 (electron) and p_4 (proton).

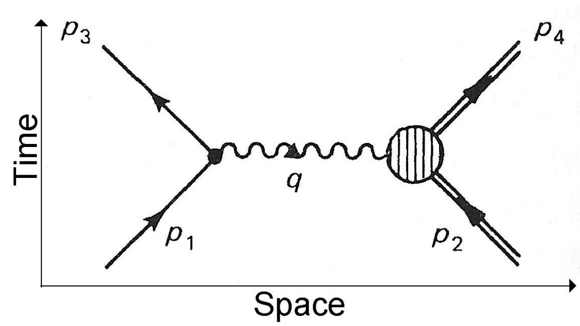

Figure 1.3: Feynman diagram for electromagnetic electron-proton scattering

The internal line is representative of a virtual photon with four-momentum q. Conservation of energy and momentum at the electron-photon vertex gives $q = p_3 - p_1$. The four-momentum transfer between the electron and the proton is defined to be:

$$Q^2 = -q^2 \tag{1.4}$$

This value relates to the energy scale $Q = \sqrt{Q^2}$ used in the previous section.

Taking the laboratory frame one has an incident electron with four momentum $p_1 = (E/c, 0, 0, p_z)$ strike an at rest proton with four-momentum $p_2 = (M_p c, 0)$. Here E is the energy of the incident electron, p_z is the momentum of the incident electron and M_p is the mass of the proton. To simplify calculations it is also assumed that the mass of the electron is zero. By use of conservation of four-momentum the equation for E' can be determined equation 1.5. The value for Q^2 can also be determined using equation 1.6.

$$E' = \frac{E}{1 + (2E/M_p)\sin^2(\theta/2)} \tag{1.5}$$

$$Q^2 = 4EE'\sin^2\theta/2 \tag{1.6}$$

Where θ is the scattering angle of the electron. These formulas will be used in later sections when discussing the tracking portion of the experiment.

1.2.2 Unpolarized cross-section

Each Feynman diagram can be calculated using the rules of Feynman Calculus and contributes a portion of the overall probability of the interaction. Higher order contributions in Quantum electrodynamics (QED) are suppressed by powers of $\alpha = 1/137$ (the fine structure constant)[2]. Ultimately the differential scattering cross-section $d\sigma/d\Omega$ may be calculated. Calculating the cross-section in this frame for the unpolarized case gives equation 1.7 [8]

$$\frac{d\sigma}{d\Omega} = \frac{\alpha^2}{4E^2\left[1 + 2\frac{E}{M_p}\sin^2\theta/2\right]\sin^4\theta/2}\left[\frac{G_E^2 + \tau G_M^2}{1+\tau}\cos^2\theta/2 + 2\tau G_M^2\sin^2\theta/2\right] \tag{1.7}$$

Where $\tau = Q^2/4M_p^2$, G_E and G_M are form factors and θ is the scattering angle of the electron.

1.2.3 Physical interpretation of form factors

The form factors G_E and G_M have an interesting physical interpretation found by taking the Breit frame or brick wall frame shown in Figure 1.4. In the Breit frame the initial four-momentum of the proton is $p_1^\mu = (E_{breit}, -\mathbf{q}_{breit}/2)$, the final four-momentum of the proton is $p_2^\mu = (E_{breit}, \mathbf{q}_{breit}/2)$. Thus the four-momentum transfer in the breit frame is $q^\mu = (0, \mathbf{q}_{breit})$ [8].

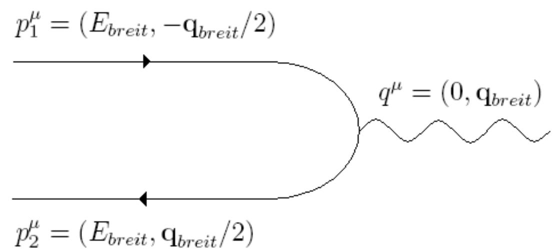

Figure 1.4: Diagram of the Breit frame

It can be shown that the form factors can be interpreted as the Fourier transforms of the protons charge density (ρ_{ch}) and magnetization density (ρ_{mag}).

$$G_E\left(Q^2\right) = \frac{4\pi}{Q}\int r dr \rho_{ch}(r)\sin Qr \tag{1.8}$$

$$G_M\left(Q^2\right) = \frac{4\pi}{Q}\int r dr \mu \rho_{mag}(r)\sin Qr \tag{1.9}$$

Where μ is the magnetic moment and the integrand is over the nuclear volume. Therefore in the limit as Q^2 goes to zero, G_E reduces to the charge of the proton and G_M reduces to the magnetic moment of the proton (in appropriate units)[8].

1.2.4 Parity violation and the weak force

In electron-proton scattering there is also another contribution due to the weak force as shown in Figure 1.5, mediated by the exchange of a virtual Z^0 boson.

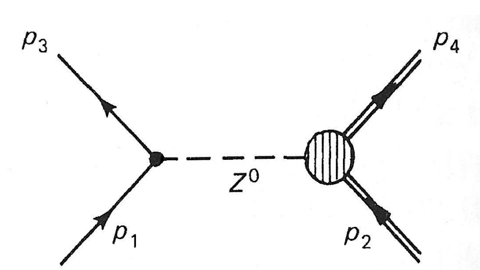

Figure 1.5: Feynman diagram for weak electron-proton scattering

Parity violation is the signature of the weak force. No other force violates parity and so parity violation can be a powerful tool in isolating the weak contribution to various interactions. The parity operator (P) is defined as performing an inversion operation. Inversion is the act of reflecting a vector through the y-axis and then performing a 180° rotation. If one operates twice with parity then the overall result is the same as that initial value.

1.2.5 Parity violating asymmetry for elastic electron-proton scattering

The Q-weak experiment makes use of a parity violating (PV) asymmetry in electron-proton scattering. This asymmetry is described by:

$$A_{PV} = \frac{(\frac{d\sigma}{d\Omega})^{+} - (\frac{d\sigma}{d\Omega})^{-}}{(\frac{d\sigma}{d\Omega})^{+} + (\frac{d\sigma}{d\Omega})^{-}} = \frac{-G_F Q^2}{4\sqrt{2}\pi\alpha}[Q_w^p + Q^2 B(Q^2)] \tag{1.10}$$

Here $(\frac{d\sigma}{d\Omega})^{+}$ is the differential cross-section for positive helicity electrons and $(\frac{d\sigma}{d\Omega})^{-}$ is the differential cross section for negative helicity electrons, Q^2 is the negative four momentum transfer squared, G_F is the Fermi constant and $B(Q^2)$ depends on nucleon, electromagnetic and strangeness form factors. The $Q^2 B(Q^2)$ factor can be accurately estimated from extrapolation of prior experimental results. Therefore by measuring A_{PV} and Q^2 we get Q_w^p.

Chapter 2

The Q-weak Experiment

2.1 Experiment Overview

The Q-weak experiment will be conducted at the Thomas Jefferson National Accelerator Facility (JLab), located in Newport News Virginia. The scheduled measurement time is 2200 hours. Measurement of Q_w^p is done by measuring the parity violating asymmetry (A_{PV}, equation 1.10) in elastic electron-proton scattering at $Q^2 = 0.03\ GeV/c^2$. The goal uncertainty in the measurement of A_{PV} is 2.5%. The goal uncertainty on Q^2 is therefore 0.5%, by equation 1.10 it can be seen that A_{PV} depends almost linearly on Q^2. This results in $(\delta A/A) = 0.5\%$ as the contribution to an overall systematic uncertainty in A_{PV} due to Q^2 determintation. Backgrounds are also to be known within 0.5% because of a similar linear relationship with A_{PV}.

2.1.1 Parity Violating Asymmetry Apparatus

Figure 2.1 [6] shows a schematic diagram of the Q-weak experiment. In the experiment a 1.2 GeV/c 180 μA electron beam is used with 85% longitudinal polarization which reverses helicity 150 times per second to minimize systematic effects related to the beam. The beam impinges on a 35cm liquid hydrogen target. Electrons scattered at an average angle of 7.9° are selected by two collimators. The electrons then enter the toroidal magnet which focusses elastically scattered electrons onto the main quartz Cherenkov bar detectors located behind a final collimator. Inelastically scattered electrons are diverted out of the Cherenkov detectors' acceptance by the toroidal field. The quartz Cherenkov bar detectors have a 200 cm x 18 cm active area and they operate in an integrating mode.

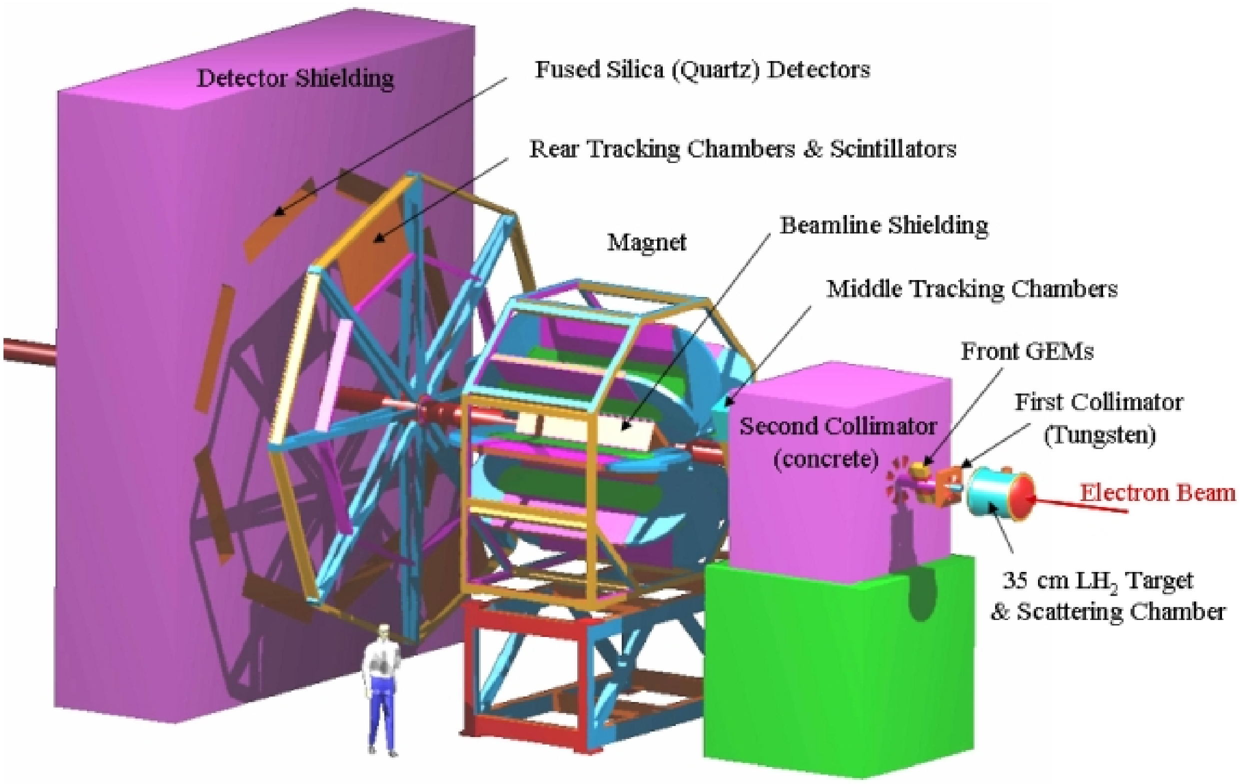

Figure 2.1: Q-weak Experiment Diagram. This Figure shows from right to left the incident electron beam, liquid hydrogen target, collimators, focusing toroidal spectrometer magnet, Cherenkov bar detectors and detector shielding. Also displayed are the tracking system detectors (GEMs and tracking chambers) that are inserted for low-current calibration. The quartz scanner is located just downstream of quartz Cherenkov bar detectors.

2.1.2 Tracking System

As mentioned previously, it is essential to precisely determine Q^2 in order to precisely determine Q_w^p from equation 1.10. A tracking system is used to make a direct measurement of Q^2 in order to make a precise determination of it's value. The tracking system detectors are slower operating detectors which operate based on ion drift followed by gas multiplication, this process can take several μs. This limits the tracking system to operation in beam currents of 1-100 nA in order to keep the rates in the detectors at manageable levels. The tracking system consists of three separate regions. Region 1 is located just after the first collimator and has gas electron multiplier (GEM) detectors (indicated by "Front GEMs" in Figure 2.1). Region 2 is located after the second collimator and contains two horizontal drift chambers (indicated by "Middle Tracking Chambers" in Figure 2.1). Region 3 is located after the toroidal magnet and contains two vertical drift chambers (indicated by "Rear Tracking Chambers" in Figure 2.1).

Determination of Q^2 and Backgrounds

Determination of Q^2 is provided if any two of the initial energy E, final energy E' and electron scattering angle θ are known. Equation (1.6) shows the relation determining Q^2 [6] and equation (1.5) shows the relation between θ and E'. The tracking chambers in region 1 and 2 provide a measurement of θ. The initial beam energy E is known to $\leq 0.1\%$ accuracy. The final energy E' can be determined from detectors in regions 2 and 3.

2.1.3 Focal Plane Scanner

Motivation

The purpose of the scanner is to extrapolate over two orders of magnitude from the calibration runs to the production runs. Similar scanning devices have been used in the E158 and Happex experiments [9], those scanners however operated in current mode in contrast to the quartz scanner for Q-weak which operates in a counting mode. In current mode, a DC current is constantly measured and variations are observed, whereas in counting mode individual events are counted to create a measurement of the rate.

General design parameters

The scanner must be radiation hard since it will be exposed to a large amount of radiation. Since quartz is radiation hard it was chosen as the radiator material for the scanner. A small active area is required so that the scanner can operate in a pulse mode even while the

Cherenkov bars are exposed to very high rates. A fast response time is also important so that the scan can be completed in reasonable time and so that the output can be correlated to the scanner's position. A final parameter is a short dead time to ensure accurate recording of the rates.

2.2 Scanner Design

A schematic of the quartz scanner light tube assembly is shown in Figure 2.2. The scanner's active area consists of the $1{\times}1$ cm^2 overlapping region of two separate $2{\times}1{\times}1$ cm^3 pieces of radiating quartz. The quartz produces light through Cherenkov radiation as explained in the next subsection.

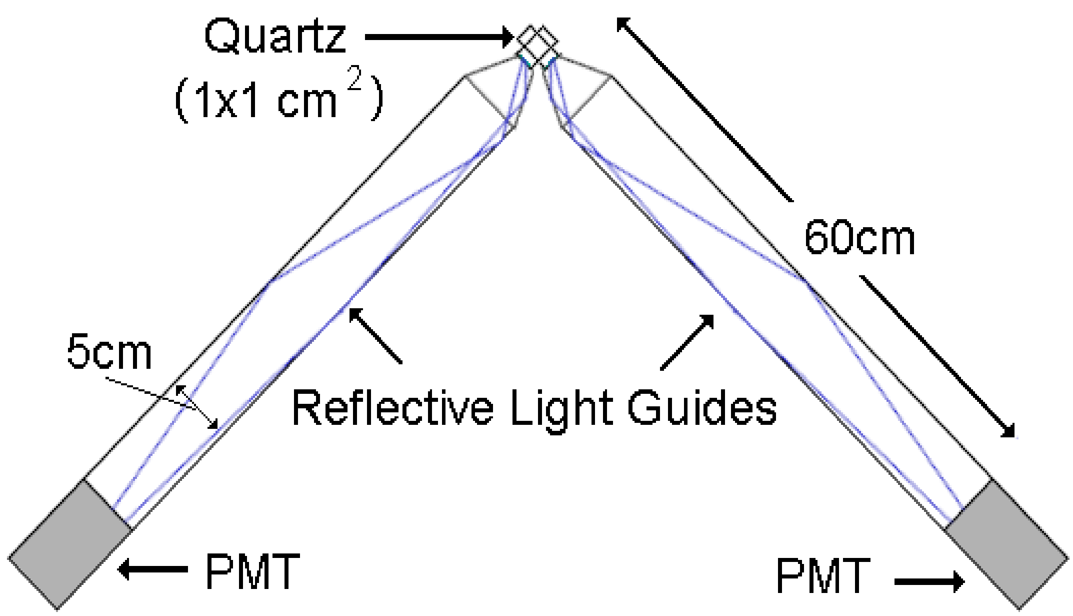

Figure 2.2: Diagram of the quartz scanner's light tube assembly

2.2.1 Cherenkov Radiation

Cherenkov radiation occurs when a charged particle moves faster than the speed of light in a medium. The threshold speed is given by [4]:

$$v_{threshold} = \beta c = c/n \tag{2.1}$$

Here n is the index of refraction and c the speed of light in a vacuum. In the cases where a particles speed exceeds this threshold an electromagnetic wave is created, similar to a sonic boom that is created when an aircraft travels faster than the speed of sound in air. A coherent conical wavefront is emitted as shown in Figure 2.3 [4] and it has a well defined angle with respect to the particles trajectory given by

$$\cos\theta_C = \frac{1}{\beta n(\omega)} \tag{2.2}$$

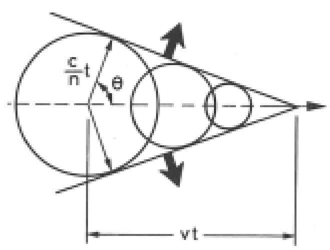

Figure 2.3: Cherenkov Radiation

2.2.2 Light tube assembly

In order to detect the light produced by the Cherenkov effect in quartz two optically isolated light guides are used. The guides are placed at a 90° angle to each other and have lengths of 60 cm. Each light guide consists of a 5 cm cone emanating from the quartz which then forms a 5 cm diameter tube which has an interior of reflective Miro 2 from Alamond Goubtt & Co. Light created in the quartz radiator is transported the length of a given light guide to a quartz window photomultiplier tube (PMT), Photonis model #2248. The length of the light guides is long enough such that when in the experiment the PMTs are out of the fiducial area of the experiment where scattered electrons would be present. The design is such that the detection of events is rapid with small dead time and the active area is small allowing the scanner to operate in a highly efficient counting mode with low background.

2.2.3 Motion assembly

In order to scan over the desired 200×18 cm^2 fiducial area of the Cherenkov bar detectors a linear motion assembly is employed. An image displaying the scanner placed on the motion assembly is shown in Figure 2.4. The motion assembly consists of x and y linear motion stages.

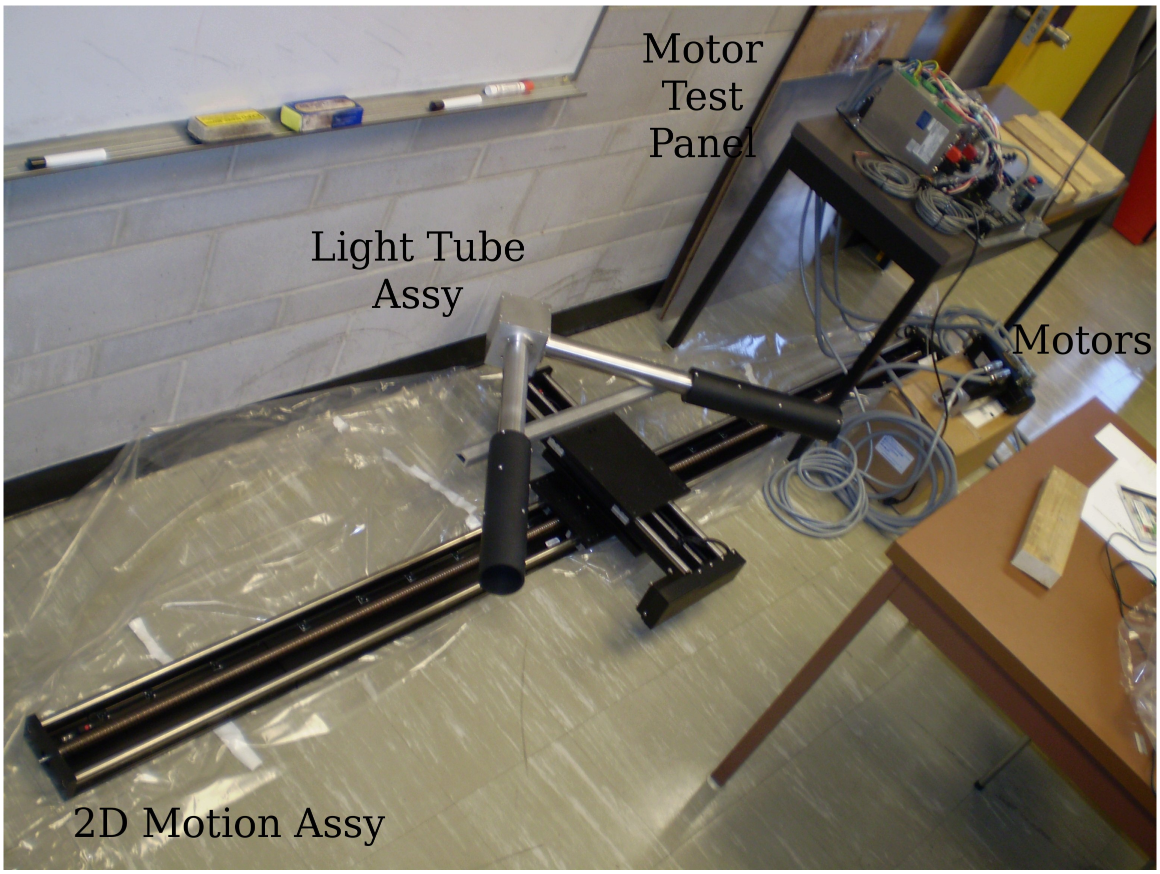

Figure 2.4: Photograph of the partially complete scanner, in the Lab at University of Winnipeg

2.3 Scanner Operation

The scanner's 1×1 cm^2 active area will be moved by the linear motion assembly until it has covered the large Cherenkov bar's area. Coincidences will be detected and correlated with the position given by the encoders on the motion assembly and used to generate a rate map characterizing the rates in a 2-D space located directly behind the Cherenkov bar detector. A schematic picture of one location of the scanner in the experiment can be seen in Figure 2.5

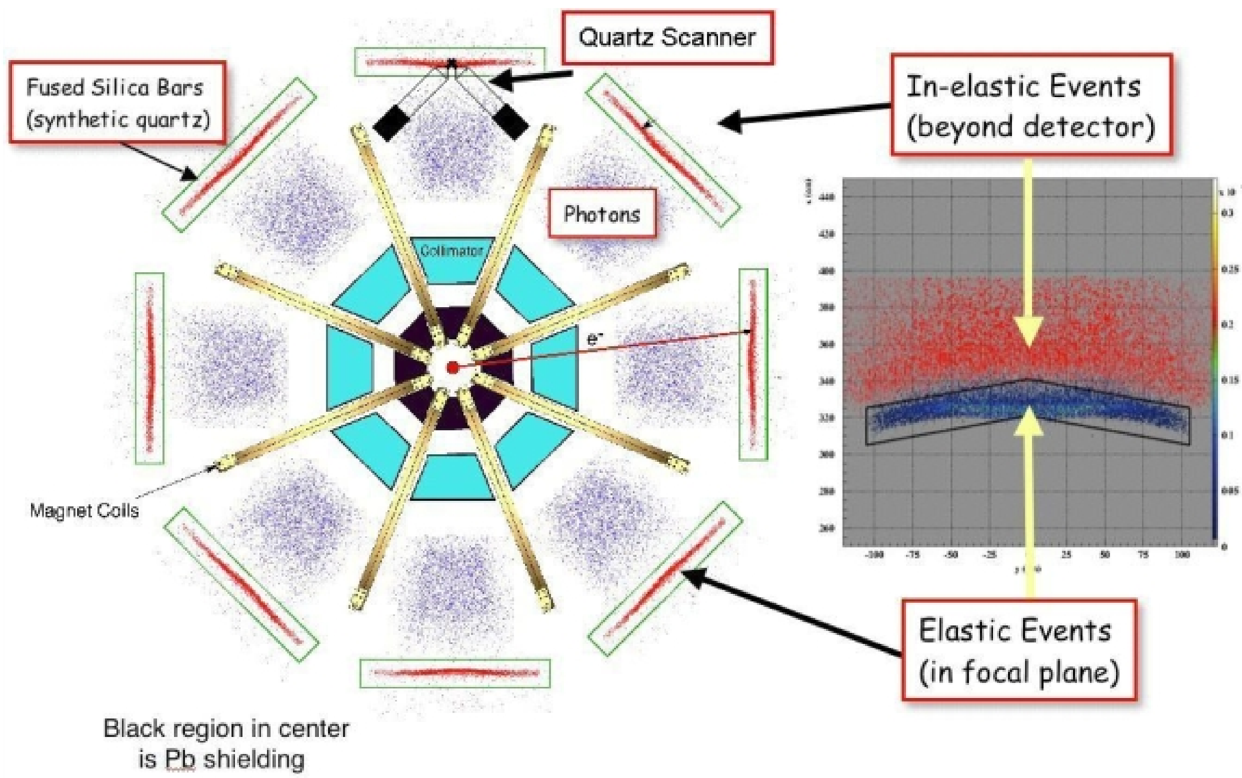

Figure 2.5: Schematic picture of the experiment showing the quartz scanner in the upper octant (Octant 1). The image on the right shows the characteristic mustache pattern formed by elastic events in the large Cherenkov bar detectors, it is this pattern which is mapped by the scanner.

2.3.1 Tracking parameter extrapolation methodology

To perform the extrapolation of Q^2 from calibration current to production current the following procedure will be used. First a 1 nA beam current is used with the full (GEM, HDC, VDC) tracking system to determine the value of Q^2 from track reconstruction. Then a beam current of 100 nA is used to cross calibrate the scanner against the vertical drift chambers in region 3. The 100 nA current is acceptable to the region 3 VDC's in terms of rate, and is large enough so that the very small active area of the scanner will see sufficiently large rate.

During production a current of 180 μA is used and the rate map from the scanner at this current is compared to those created at 100nA. Confidence in this comparison depends on several systematic effects in the quartz scanner which are rate sensitive.

2.3.2 Systematic effects on extrapolation

To properly implement the quartz scanner in the Qweak experiment systematic effects which affect the confidence in the rate map must be examined and quantified. These effects are accidental coincidences, backgrounds and dead time.

Accidental Coincidence

A coincidence technique is used to signify the passage of an electron through the scanner's active area. To cause a coincidence the electron must produce light in both pieces of quartz and that light must be detected by the photomultiplier tubes (PMTs). An accidental coincidence occurs when two uncorrelated particles happen to give a signal to each PMT in a time window τ. For example an electron can pass through one of the light guides creating scintillation photons in the air core of the light guide while within the coincidence time window τ another electron passes through the other tube producing a signal in it. The rate of accidental coincidences A can be calculated using [4]:

$$A \cong \tau N_1 N_2 \tag{2.3}$$

Where N_1 is the singles rate in tube 1 and N_2 is the singles rate in tube 2. Also assumed is that N_1 and N_2 are stable in time. The singles rate is the rate seen by one PMT or the other. The coincidence rate differs in that both PMTs must each see an event within the coincidence time window τ. Accidental coincidences tend to increase the detected coincidence rate erroneously by an amount equal to A. High rate coincidence experiments must therefore minimize and correctly account for this systematic effect.

Dead time

Dead time is the time in which a detector is unable to respond due to a finite recovery time after a prior detection. This occurs when two distinct particles strike the detector within a time interval τ_{dt} and hence can not be resolved. When this occurs the detector misses the second event resulting in a detected rate which is lower than the actual rate. Dead time is an intrinsic property of a detector. The relationship between true rate R_{true} and the measured rate $R_{measured}$ is shown in equation 2.4

$$R_{true} = \frac{R_{measured}}{1 - \tau_{dt} R_{measured}} \tag{2.4}$$

The effect of dead time is to decrease the measured rates artificially from the desired true rate.

2.3.3 Other uses for the scanner

The scanner can also be used in background determination. Backgrounds can be created by inelastically scattered electrons and scattering of electrons from other objects in the experiment such as the coils, as well as the general background that exists in the experimental hall. These backgrounds can produce light in the quartz scanner as well as in the large quartz Cherenkov bars. These backgrounds can be partially characterized by the quartz scanner. Backgrounds are detrimental since they provide signal which is not related to elastic electron-proton scattering. The advantage of the scanner in this regard is that its scan range is larger in size than the fiducial area of the tracking system, particularly the region 3 VDC's. The scanner could, for example, scan well into the inelastic region indicated in Figure 2.5, so that extrapolation of inelastic contamination of the elastic focus could be inferred through use of a fitting technique.

2.3.4 Scan rate and pattern

The scanning pattern and scanning speed are important variables since they effect the number of counts used to determine the rate. The variables of interest in determining scan pattern and rate are the helicity reversal speed of 150 Hz, the coordination with output of location from the motion assembly and statistical concerns.

Chapter 3

Simulations

3.1 Overview of Simulations

The simulations of the scanner in the experimental setup were coded in c++. The simulations use the Monte Carlo method to calculate the rate values for each location on the rate map. The methods used in simulations are explained in the following sections.

3.1.1 Input rate map

The input to the simulation consisted of a text file containing the coordinates and rates in the focal plane of the Q-weak spectrometer (at the site of a quartz Cherenkov bar detector). The initial rate map was created by a simulation of the Q-weak experiment at 180μA [10]. The text file was read into the simulation and was referenced in order to determine the rate at any location. The rate map was binned into 1×1 cm squares which cover the full 200×18 cm^2 large quartz bars. The input rate map is shown in Figure 3.1, the colors represent the rate in units of MHz/cm^2. Note that in this Figure, and in several that follow, the bins have a definite aspect ratio, i.e. each rectangle represents a 1×1 cm^2 bin.

3.1.2 Coordinate transforms

The coordinates and single tube geometry in the simulation are shown in Figure 3.2. The main coordinate system is a cartesian coordinate system with it's origin in the lower middle of the 200×18 cm^2 active area of the Cherenkov bar detectors. A primed coordinate system

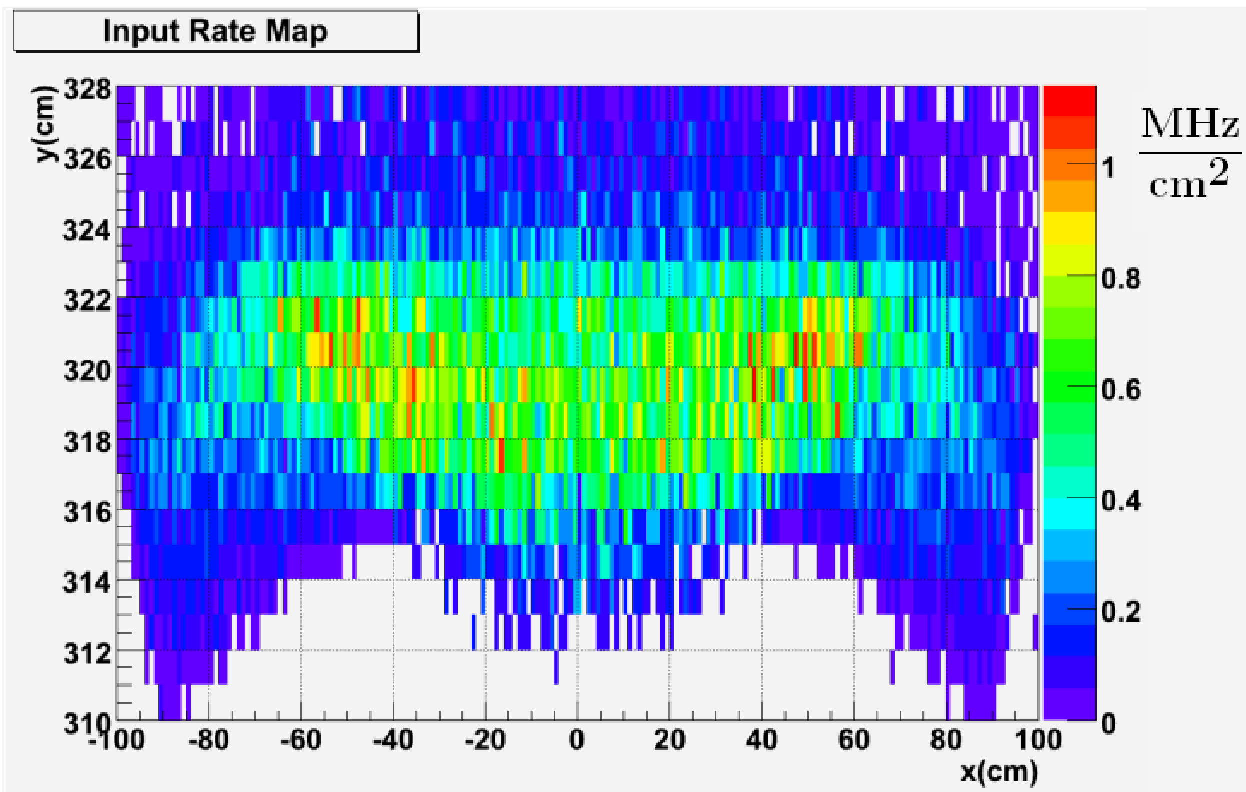

Figure 3.1: Input rate map for current of 180 μA, note the aspect ratio is skewed, each rectangle represents a $1{\times}1$ cm^2 bin, the color map represents the MHz/cm^2

is created for each tube with its origin at the center of the quartz furthest from the PMT as shown. The transformation into this primed frame is given by equations 3.1 and 3.2. To define the coordinate system of the tube shown the x' transform is reflected through the y-axis, in this way both tubes had their own coordinate systems.

$$x' = -\left[(x - q_x)\sin\theta + (y - q_y)\cos\theta\right] \tag{3.1}$$

$$y' = -(y - q_y)\sin\theta + (x - q_x)\cos\theta \tag{3.2}$$

Where x and y are the coordinates of the point to be transformed and (q_x,q_y) is the location of the center of the quartz in the unprimed system.

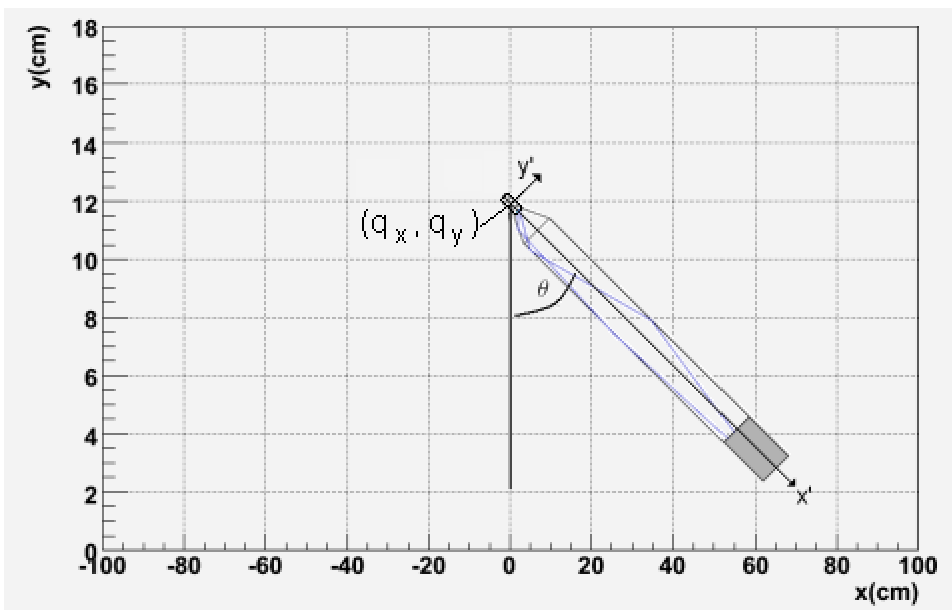

Figure 3.2: This schematic shows the coordinate system for the rate map and the primed system for one scanner tube, the location of the center of the quartz in the unprimed system is defined by the point (q_x,q_y). Note that two different aspect ratios have been used for the two systems in the interest of clarity.

3.1.3 Individual light tube response function

To determine the light output from an electron striking various locations on the scanner a light response function was used. If the electron struck the quartz it was taken that 10 photoelectrons were produced, striking the cone produced 0.1 photoelectrons and striking the tube produced 0.01 photoelectrons. These values for the number of photoelectrons were determined from a simulation of tube response [7] and refer to the mean number of photoelectrons ($N_{p.e.}$) detected by the PMT for the relevant tube. For these simulations it was assumed the response was uniform in y'. This is an oversimplification of the response of a cylindrical light guide and could be modified in future work.

Using the method described in the next section to determine efficiencies a plot of the efficiency weighted rate for one tube was plotted, see Figure 3.3.

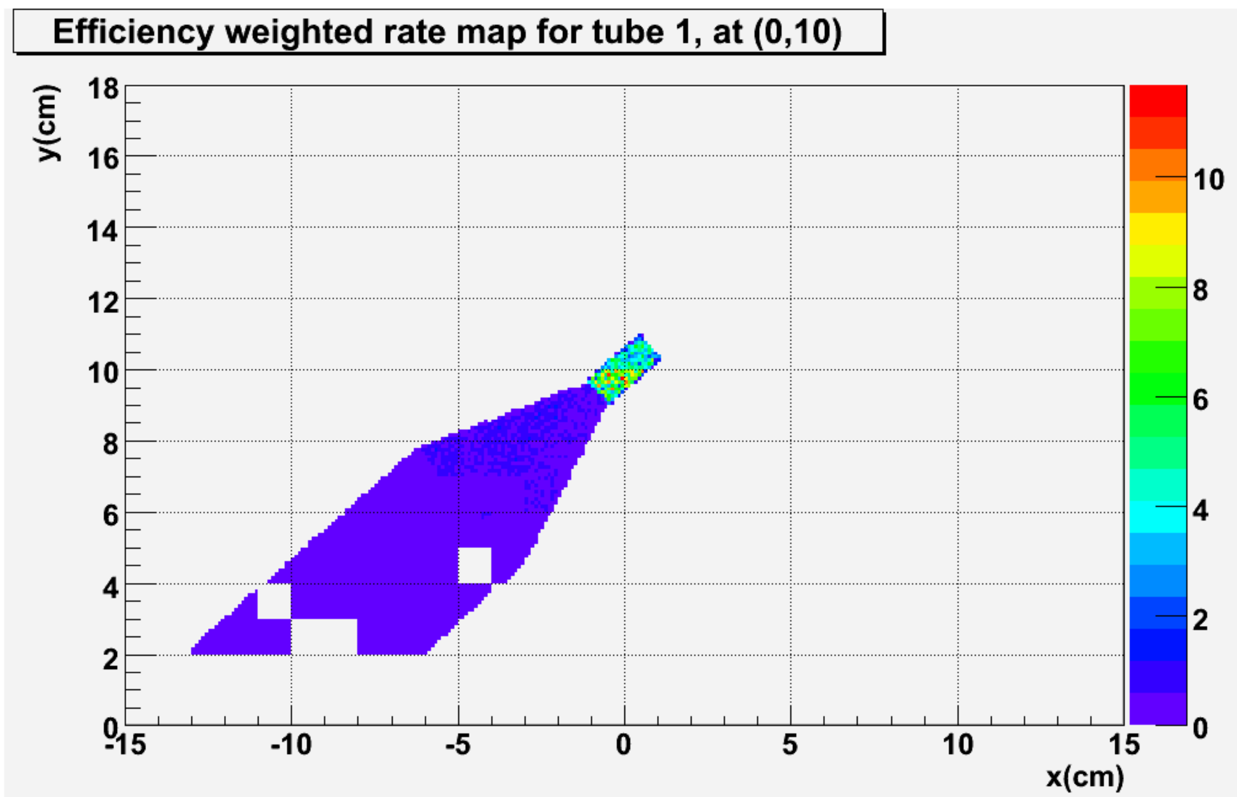

Figure 3.3: The efficiency weighted rate for a tube at the coordinate (0,10), the color scale was arbitrary chosen to effectively demonstrate the tube response

3.1.4 Poisson distribution

The Poisson distribution can be used to find the probability of detecting γ photoelectrons for given event given the mean number of photons created in the event ($N_{p.e.}$). The Poisson distribution is given in equation 3.3

$$P(\gamma) = \frac{N_{p.e.}^{\gamma} e^{-N_{p.e.}}}{\gamma!} \tag{3.3}$$

By subtracting from 1 the terms for $\gamma >$ 1,2,3 the efficiencies for thresholds 1,2 and 3 are given. Threshold one gives the probability of seeing at least one photoelectrons given the number created, threshold two means seeing at least 2 photoelectrons and threshold 3 at least 3 photoelectrons. Using this result equation 3.4 determined the efficiency for each point based on the number of photoelectrons.

$$\epsilon_{N_{thr}}(\geq N_{thr}) = 1 - \sum_{\gamma=0}^{N_{thr}-1} P(\gamma; N_{p.e.}) \tag{3.4}$$

Where γ is the number of photoelectrons detected by the tube, $N_{p.e.}$ is the number created in the tube and N_{thr} is the threshold number. For threshold 3 the efficiency (ϵ_3) becomes:

$$\epsilon_3 = 1 - e^{-N_{p.e.}} - (N_{p.e.})\, e^{-N_{p.e.}} - \frac{1}{2}(N_{p.e.})^2 e^{-N_{p.e.}} \tag{3.5}$$

3.2 Description of the Monte Carlo method

The goal of the code is to integrate the rate seen by the quartz scanner for every 1x1 cm^2 bin that it scans over in the course of scanning the active area of the Cherenkov bar detectors. To perform this integral a Monte Carlo method was used.

3.2.1 Monte Carlo principle for a single scanner tube

Consider a particular location for the scanner (q_x, q_y). In the simulation an event consists of generating a random point (x,y) within the 200×18 cm^2 area described by the unprimed coordinate system. The rate for the random point is looked up in the input rate map. The point is then transformed into the primed detector coordinate system as described in equations 3.1 and 3.2. From this information it is determined if the point is within the scanners area and what the corresponding efficiency is. If the location was outside of the scanners area it was given a zero efficiency value. This process of random point generation is then repeated. The singles rate for each tube and the coincidence rate was summed for every randomly chosen point (x,y). Similar efficiency weighted singles rates and coincidence rates were also found. After the completion of many events the results for a given rate of interest was calculated using equation 3.6.

$$R = \frac{AR_s}{n} \tag{3.6}$$

Where R is the rate of interest, A is the area in which random points were chosen, R_s is the summed rate and n is the number of random points chosen. The value R is the solution to the rate integral for a single (q_x, q_y)which was the goal of the Monte Carlo.

3.2.2 Simulation of a scan

The completion of a scan in the simulation consists of moving the scanner to every $1{\times}1\text{cm}^2$ bin and performing the calculation described in the previous section to determine the rate for each location. Figure 3.4 displays the result of such a scan with the threshold set as threshold 1 and the beam current being 180 μA. This figure can be compared to the input rate map shown in Figure 3.1.

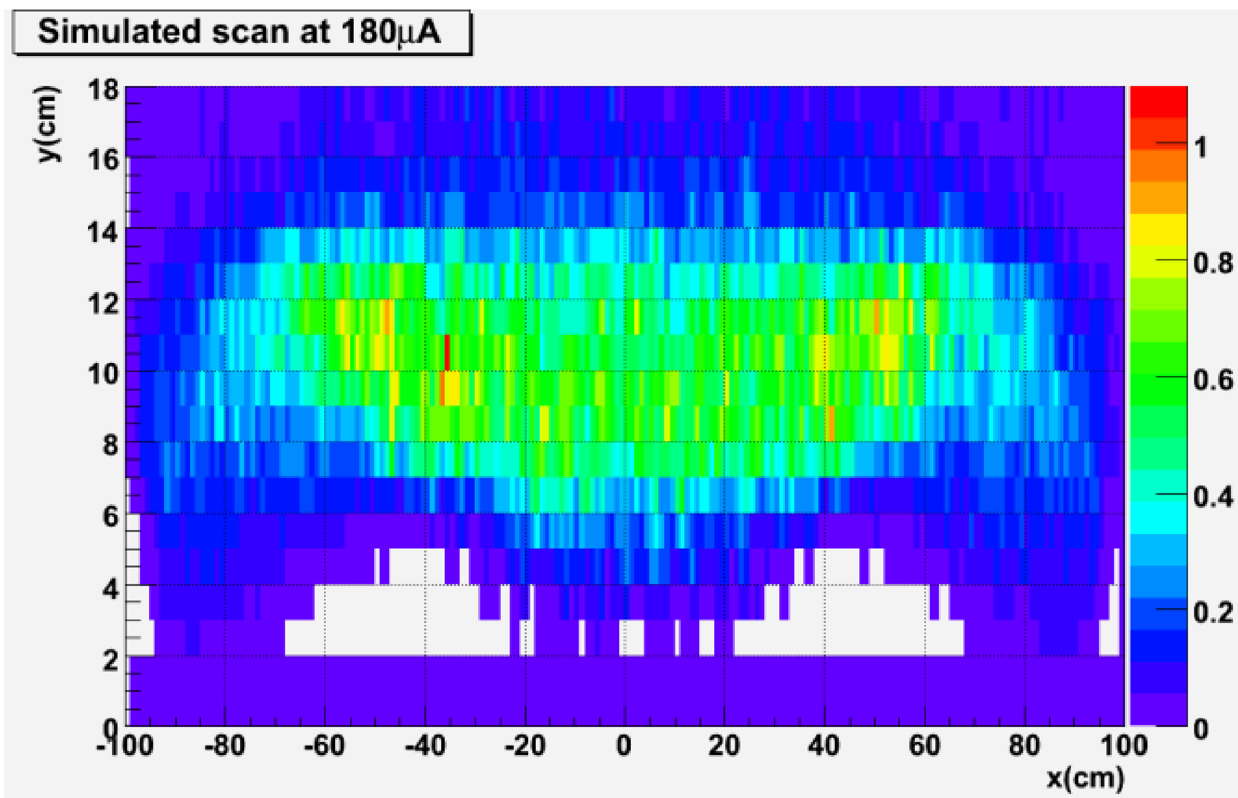

Figure 3.4: The result of a scan at threshold 1 and beam current 180μA, the color map represents MHz/cm^2

3.3 Code capabilities

3.3.1 Variability of threshold

For the purposes of the simulations presented in this thesis the method discussed in the Poisson distribution section was implemented to provide 3 threshold values corresponding to observing at least 1,2 or 3 photoelectrons respectively.

3.3.2 Variability of beam current

The input rate map is given for a beam current of 180 μA, to have the current change in the simulation the input values must simply be multiplied by the appropriate factor. For example to go from 180 μA to 100 nA one would divide by 1800.

3.3.3 List of variables

Here is a list of variables available in the simulation output data file:

- q_x coordinate
- q_y coordinate
- efficiency in tube 1
- efficiency in tube 2
- singles rate in tube 1
- singles rate in tube 2
- efficiency weighted singles rate in tube 1
- efficiency weighted singles rate in tube 2
- perfect coincidence rate
- efficiency weighted coincidence rate

In addition to the above, event level information can also be accessed in special runs where the scanner location is fixed. This can be useful for debugging purposes as well as identifying problems with the light tube design. From now on we use x and y to denote q_x and q_y in plots and notation.

Chapter 4

Results

Throughout this section there are displayed various plots in which the aspect ratio is skewed in the vertical direction. When reading these plots note that each rectangular bin actually is representative of a 1×1 cm^2 bin. The units which determine the color values in the plots are those of $\frac{d^2R}{dxdy}$, most commonly in MHz/cm^2. As well when referring to tubes 1 and 2, tube 1 is the tube which is in the negative x region when the scanner is located in the center of the unprimed coordinate system, refer to Figure 3.2 which shows tube 2. A “tube” constitutes one of the pieces of scintillating quartz and a light guide leading to a PMT.

4.1 Study of accidental coincidences

As discussed in the systematic effects section, accidental coincidences are an important effect which needs to be characterized. The goal of this study was to investigate the effect of threshold and beam current on the accidental coincidence rate. To do this the accidental coincidence rate was calculated and expressed as a percentage of the true coincidence rate for a detector with perfect efficiency and time resolution.

4.1.1 Singles rate map

The formula for percent accidental coincidences involves the use of the singles rate. A plot of the singles rate in tube 1 is shown in Figure 4.1

From this plot note that the maximum singles rate is 2.5 MHz. Trends follow the input rate map (Figure 3.1), but rates at approximately 14-18 cm are drastically increased due to

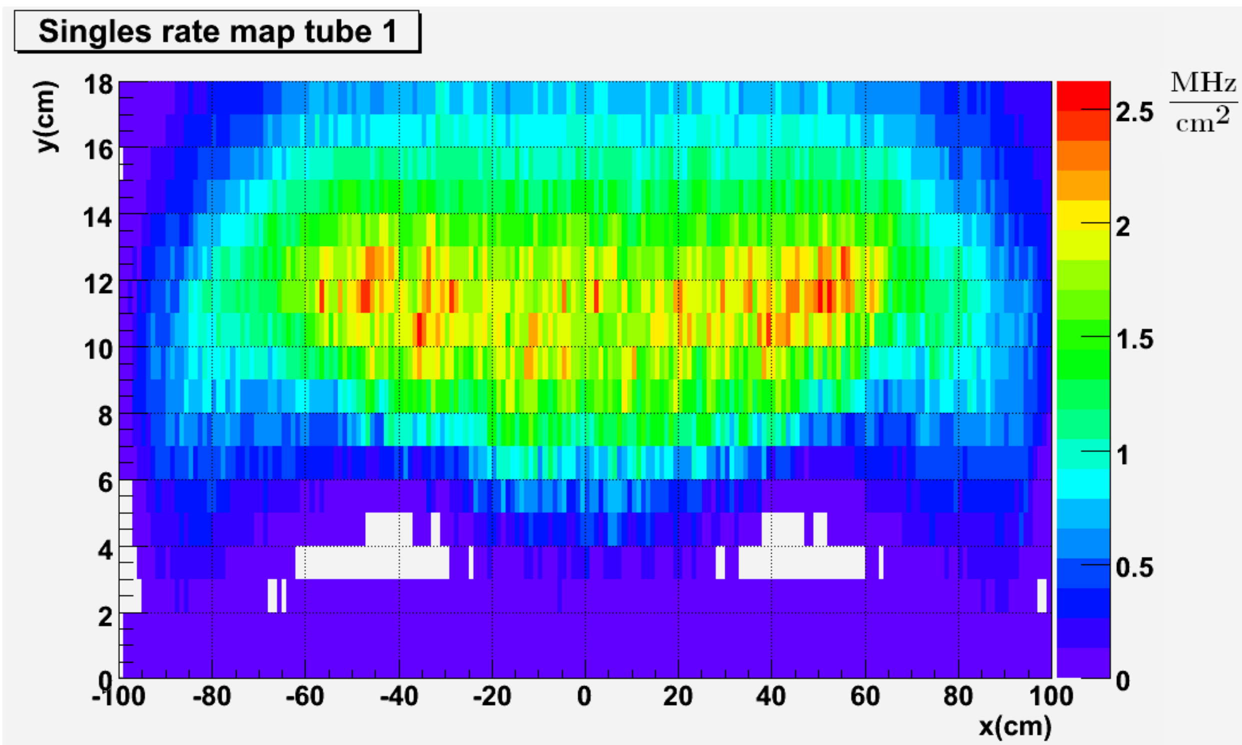

Figure 4.1: Threshold 1 rate map showing the singles rate in tube 1 at 180 μA, the color map represents MHz/cm^2

backgrounds arising from the air-core light guide.

4.1.2 Estimate of accidentals

The formula for percent accidental coincidences involves the use of the singles rates in both tubes. Since the rate map is nearly symmetric an estimate for accidentals can be made using the singles rate from one of the tubes, in this case tube 1. From Figure 4.1, the maximum singles rate in tube 1 is 2.5 MHz. Using equation 2.3 with $\tau = 0.02\mu s$ one gets A = 0.125 MHz. This corresponds to 5% of the measured rate.

4.1.3 Accidental coincidence map threshold 1

Performing the same calculation using the rates from each tube and results for the whole rate map gives an accidental coincidence rate map. To compare the accidental coincidence map to the true coincidence rate map the ratio of the two was taken and expressed as a percentage. The result is shown in Figure 4.2. It can be seen that the percent accidentals is typically 30 % in regions of high rate.

The high singles rates observed for threshold 1 are created by large backgrounds in the regions where the average number of created photo electrons ($N_{p.e.}$) is 0.01. Raising the threshold should suppress the accidental coincidence rate.

4.1.4 Accidental coincidence map for thresholds 2 and 3

The suppression of accidentals rate is observed in the results for thresholds 2 and 3 displayed in Figures 4.3 and 4.4 respectively. The maximum percentage of accidental coincidences is 7% for threshold 2 and 6% for threshold 3.

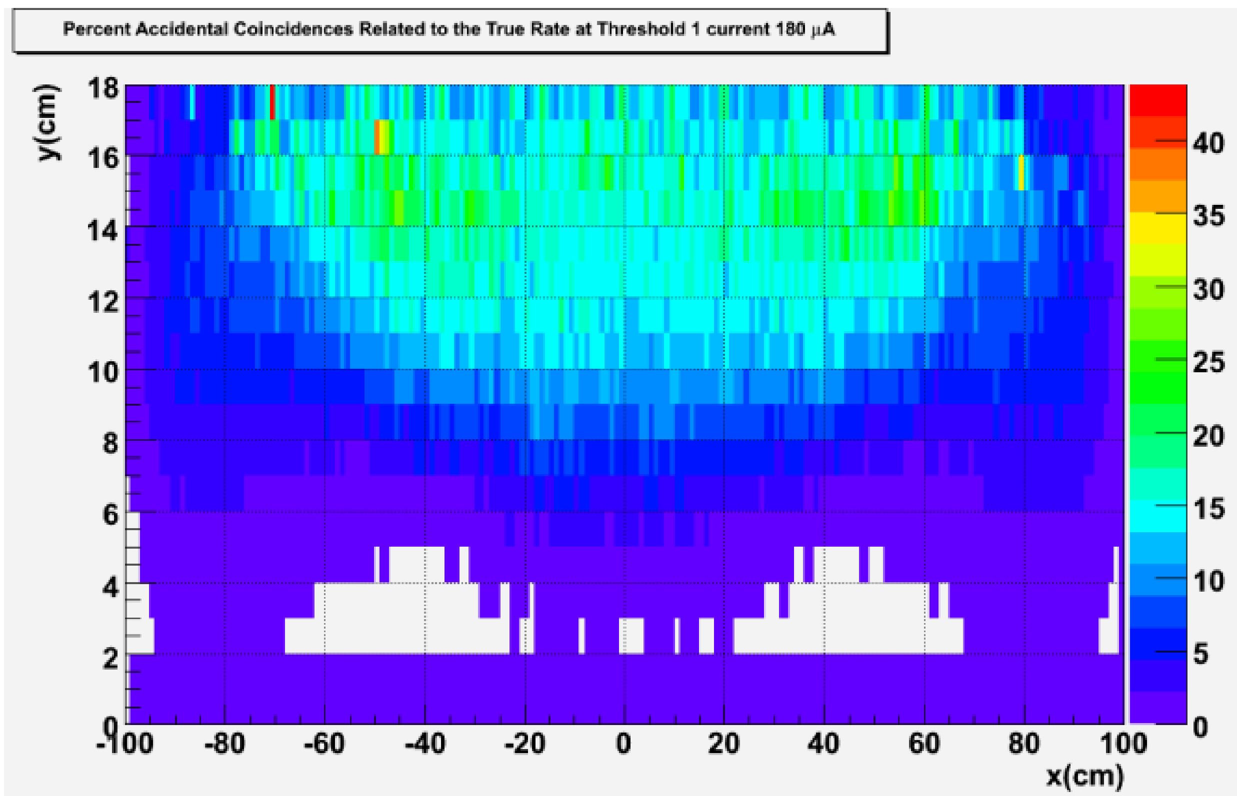

Figure 4.2: Threshold 1 map showing percent accidentals at 180 μA, the color map represents the % of accidental coincidences relative to the perfect coincidence rate

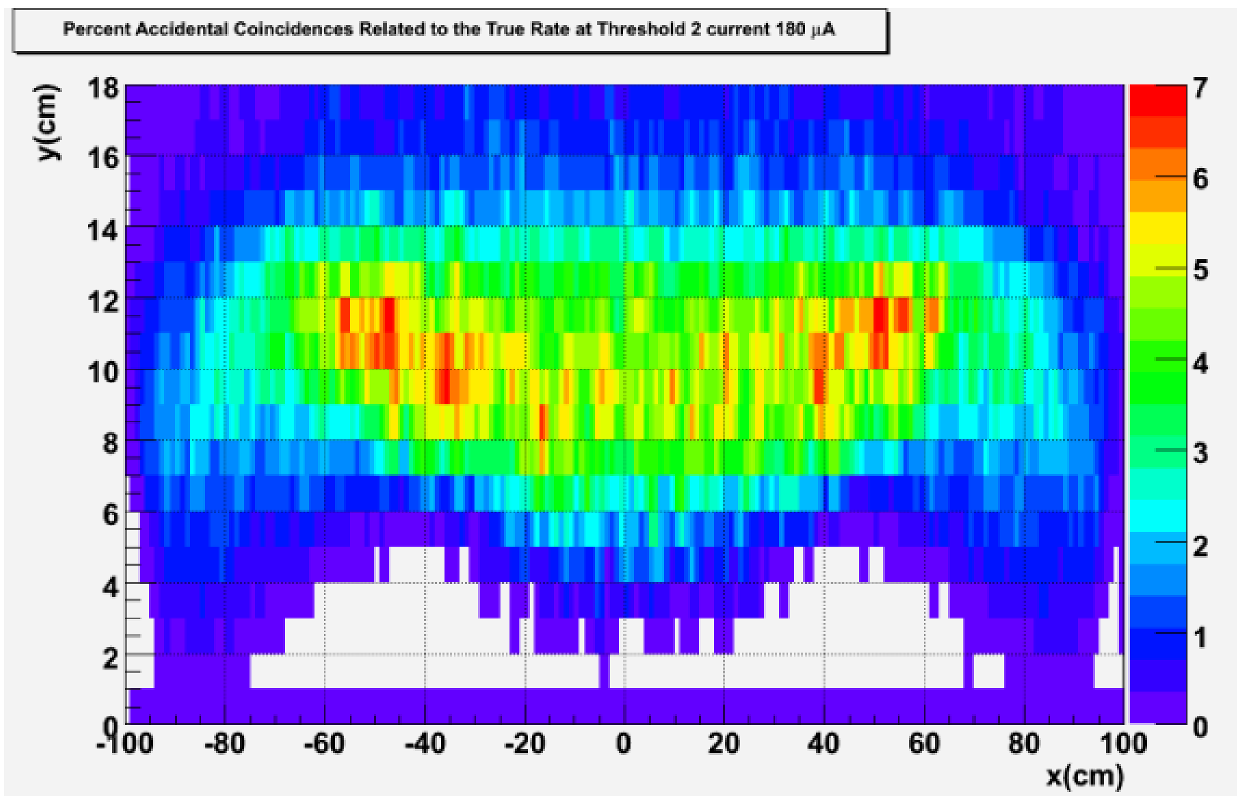

Figure 4.3: Threshold 2 map showing percent accidentals at 180 μA, the color map represents the % of accidental coincidences relative to the perfect coincidence rate

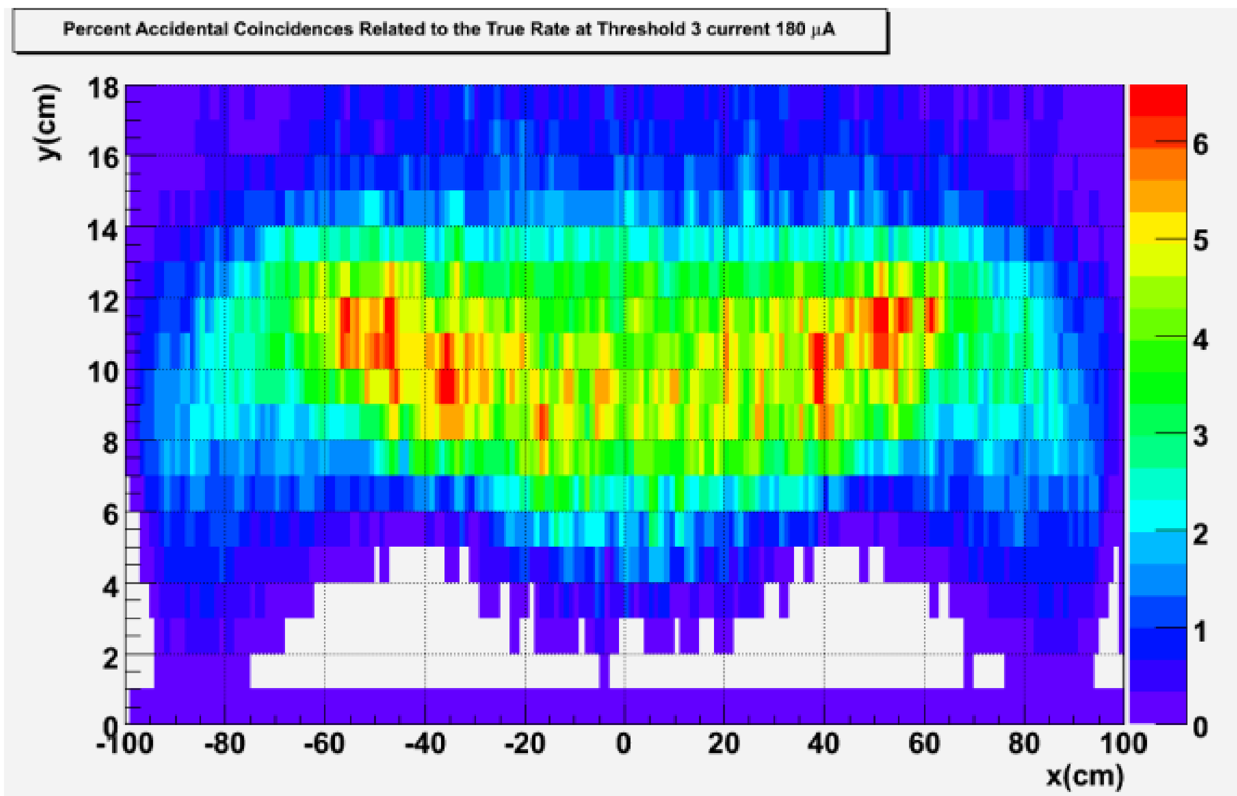

Figure 4.4: Threshold 3 map showing percent accidentals at 180 μA, the color map represents the % of accidental coincidences relative to the perfect coincidence rate

4.1.5 100 nA accidental coincidence map

Also of interest was how the accidental coincidence map would translate to a beam current of 100nA. Figure 4.5 shows the accidental coincidence map as a percentage of perfect coincidences for threshold 3 and beam current 100nA. As expressed the percentage of accidentals is much lower at 100 nA than at 180 μA, reaching only to 0.02% of the true coincidence rate.

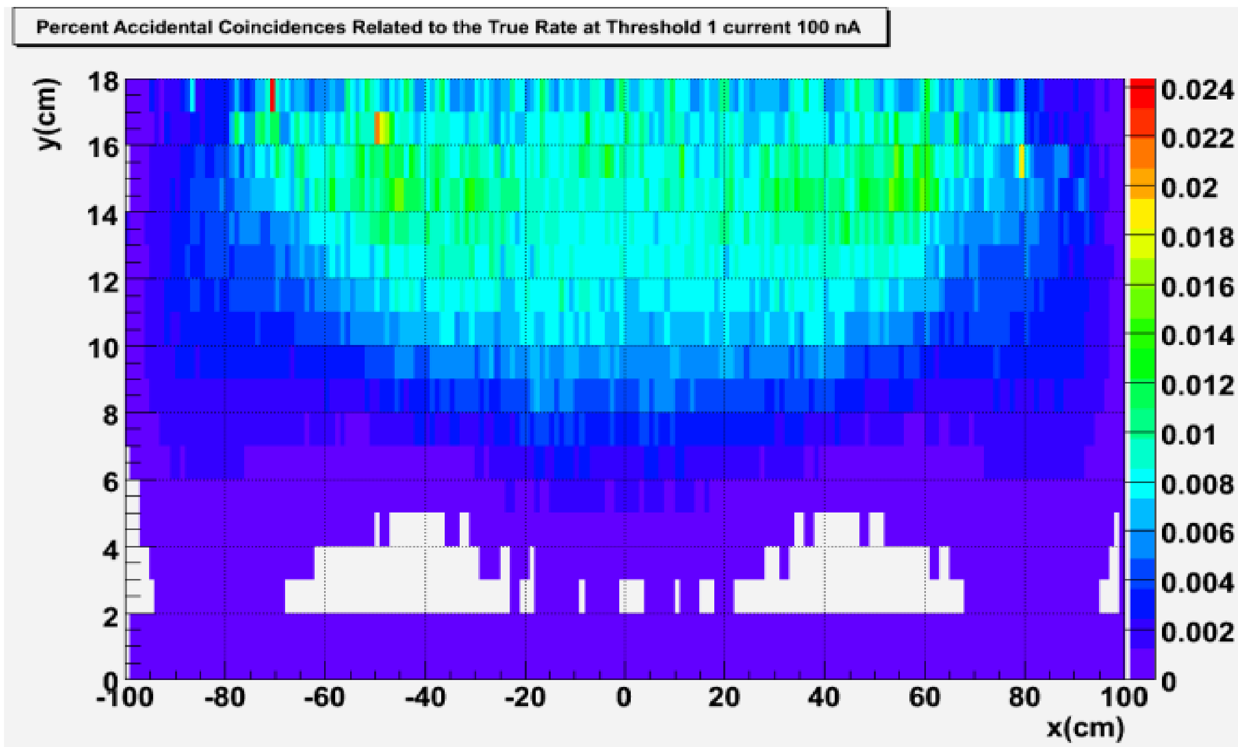

Figure 4.5: Threshold 1 map showing percent accidentals at 100 nA, the color map represents the % of accidental coincidences relative to the perfect coincidence rate

4.2 Relationship between coincidence efficiency and accidental coincidence rates

It was found that by increasing the threshold the accidental coincidence rate fell. The following table displays the relationship between threshold, efficiency (from equation 3.4) and accidental coincidence rates (from previous section).

Threshold	$\epsilon\,(10)^2$	max % accidental coincidences
1	0.9999080	30%
2	0.9990014	7%
3	0.9944689	6%

From the above table it is seen that the ideal threshold would be threshold 2. This is because it provides a significantly lower percentage of accidental coincidences when compared to threshold 1. Also when compared to threshold 3, threshold 2 provides a higher accepted rate and a comparable percent accidental coincidence rate making threshold 2 the best option.

4.3 Dead time

Dead time for the scanner can be determined from the singles rate for one tube. Since the rate map is approximately symmetrical the dead time for one tube during a scan would be near identical to that of the other tube. Using equation 2.4 the dead time in a single tube can be estimated in a location of highest rate. The maximum is chosen since that is where the effects of dead time will be greatest. Using the singles rate map in Figure 4.1 the highest singles rate is found to be 2.5 MHz and taking $\tau_{dt} = 0.02\ \mu s$ corrected singles rate is 2.63 MHz. This means that the dead time correction represents 5% of the detected singles rate.

4.4 Comments on scan rate

The scan rate depends on several variables which are explored in this section.

Statistical considerations

In order to obtain statistically significant results for the scanner the speed must be such that a sufficient number of counts are determined for each location the scanner scans. This number is effected by the rate and threshold value of the scanner. The higher the rate the less time required to acquire sufficient counts. Also the lower the threshold the less time needed to acquire sufficient results, but as seen earlier this lowering of threshold increases the occurrences of accidental coincidence.

Variation of rate with respect to position

As the scanner moves through a scan it is essential that the measured rates can be linked to the location of the scanner. In locations with high variation in rate with position it may be required to slow the scan down to ensure accurate creation of the rate map. Slopes of measured rate (R_{meas}) vs position in x an y ($\partial R_{meas}/\partial x$ and $\partial R_{meas}/\partial y$), locations of rapidly changing rate can be recognized.

Variability of Q-weak parameters with time

During the run time of the experiment, parameters will shift. For example the beam may shut off or change location causing a change in the observed scanner coincidence rate. To ensure confidence in the results of a scan the scan time should be kept under 20 minutes. This should ensure that the experimental parameters will not have shifted so significantly that the scan will not be useful.

Chapter 5

Conclusion

The Q-weak experiment, its motivation and the quartz scanner detector for the experiment were presented. The motivation of the scanner was discussed with a focus on the extrapolation of Q^2 to production current. A custom simulation of the detector's operation was coded and was used to investigate runtime parameters for the scanner. Results suggest that accidental coincidence rates are strongly dependent upon the beam current and will need to be accounted for, or if deemed unacceptable, the scanner redesigned to reduce the accidental coincidence rate. Nonetheless, an acceptable solution to minimize accidental coincidence rate while maximizing efficiency was found. Further investigations are possible with this code that will help determine what the correction methodology will be when the scanner is installed in the experiment.

Bibliography

[1] D. Armstrong *et al.* (the Q-weak collaboration), "The Q^P_{Weak} Experiment: A search for new Physics at the TeV Scale via a Measurement of the Protons Weak Charge ", (2004),(unpublished).

[2] David J. Griffiths, "Introduction to Elementary Particles", WILEY-VCH Verlag GmbH & Co. KGaA, Weinheim (2004).

[3] Qweak website, http://www.jlab.org/qweak/ (2008).

[4] W.R. Leo, "Techniques for Nuclear and Particle Physics Experiments", Springer-Verlag Berlin Heidelberg (1994).

[5] J. Erler, A. Kurylov and M. J. Ramsey-Musolf, Phys. Rev. D **68**, 016006 (2003).

[6] D. Armstrong *et al.* (the Q-weak collaboration) ,"Update for Q-weak", prepared for JLab PAC Jeopardy process, (2008),(unpublished).

[7] Jie Pan, private communication.

[8] Bradley R. Plaster, The Neutron Elastic Form Factor to $Q^2 = (1.45 \text{ GeV/c})^2$, PhD thesis, Massachusetts Institute of Technology (2004),(unpublished).

[9] R. S. Hicks *et al.*, Nucl. Instrum. Meth. A **553**, 470 (2005).

[10] J. Mammei, private communication.